Title

Evaluation of the geometric accuracy of computed tomography and microcomputed tomography of the articular surface of the distal portion of the radius of cats.

Journal

American Journal of Veterinary Research, 80(10)

ISSN

0002-9645

Authors

Webster, Caroline E
Marcellin-Little, Denis J
Koballa, Erin M
et al.

Publication Date

2019-10-01

DOI

10.2460/ajvr.80.10.976

Peer reviewed

Evaluation of the geometric accuracy of computed tomography and microcomputed tomography of the articular surface of the distal portion of the radius of cats

Caroline E. Webster PhD
Denis J. Marcellin-Little DEDV
Erin M. Koballa DVM
Jonathan W. Stallrich PhD
Ola L. A. Harrysson PhD

Received April 6, 2019.
Accepted May 6, 2019.

From the Edward P. Fitts Department of Industrial and Systems Engineering, College of Engineering (Webster, Harrysson), and the Department of Statistics, College of Sciences (Stallrich), North Carolina State University, Raleigh, NC 27695; and the Department of Clinical Sciences, College of Veterinary Medicine, North Carolina State University, Raleigh, NC 27607 (Marcellin-Little, Koballa). Dr. Marcellin-Little's present address is Department of Veterinary Surgical and Radiological Sciences, School of Veterinary Medicine, University of California-Davis, Davis, CA 95616. Dr. Koballa's present address is North Mecklenburg Animal Hospital, 19126 Statesville Rd, Cornelius, NC 28031.

Address correspondence to Dr. Marcellin-Little (djmarcel@ucdavis.edu).

OBJECTIVE
To evaluate accuracy of articular surfaces determined by use of 2 perpendicular CT orientations, micro-CT, and laser scanning.

SAMPLE
23 cat cadavers.

PROCEDURES
Images of antebrachia were obtained by use of CT (voxel size, 0.6 mm) in longitudinal orientation (CT_{LO} images) and transverse orientation (CT_{TO} images) and by use of micro-CT (voxel size, 0.024 mm) in a longitudinal orientation. Images were reconstructed. Craniocaudal and mediolateral length, radius of curvature, and deviation of the articular surface of the distal portion of the radius of 3-D renderings for CT_{LO}, CT_{TO}, and micro-CT images were compared with results of 3-D renderings acquired with a laser scanner (resolution, 0.025 mm).

RESULTS
Measurement of CT_{LO} and CT_{TO} images overestimated craniocaudal and mediolateral length of the articular surface by 4% to 10%. Measurement of micro-CT images underestimated craniocaudal and mediolateral length by 1%. Measurement of CT_{LO} and CT_{TO} images underestimated mediolateral radius of curvature by 15% and overestimated craniocaudal radius of curvature by > 100%; use of micro-CT images underestimated them by 3% and 5%, respectively. Mean ± SD surface deviation was 0.26 ± 0.09 mm for CT_{LO} images, 0.30 ± 0.28 mm for CT_{TO} images, and 0.04 ± 0.02 mm for micro-CT images.

CONCLUSIONS AND CLINICAL RELEVANCE
Articular surface models derived from CT images had dimensional errors that approximately matched the voxel size. Thus, CT cannot be used to plan conforming arthroplasties in small joints and could lack precision when used to plan the correction of a limb deformity or repair of a fracture. (*Am J Vet Res* 2019;80:976–984)

The 3-D geometry of bones and joints can be determined from MRI or CT images, and MRI-based 3-D models of articular surfaces have been reported.[1,2] Geometric accuracy of CT images have been described in several studies, including studies that focused on cortical thickness[3] and geometry of the articular surface.[4–7] Accuracy of CT, cone-beam CT, and micro-CT is influenced by several factors, including beam orientation relative to the scan surface and slice thickness.[3] An increase in the popularity of additive manufacturing has led to the common use of CT data to create 3-D or physical models. Accuracy of additive manufacturing models produced from CT-derived 3-D models has been evaluated with a focus on CT scan variables and CT scan segmentation variables.[8,9] Imaging with CT has been used to assess the shape and relative position of bones,[10] estimate joint loads,[11–13] conduct computational modeling of articular contact,[14,15] assess pathological changes in joints,[16,17] and plan surgical procedures.[18]

In addition to evaluation by use of CT, the 3-D geometry of articular surfaces has been evaluated by use of several methods that rely on ionizing radiation, line-of-sight scanning, or coordinate measurements. Stereophotogrammetry has been used to evaluate the shape of cartilage and subchondral bone.[19] Laser coordinate measuring systems have also been used to evaluate bone shape[20] and symmetry.[21] Studies conducted to evaluate accuracy and validation of CT have involved the use of coordinate measuring systems as the criterion-referenced standard for the knee joints,[22] phalanges,[23] and vertebral column[24] of humans.

Our research group has focused on designing limb-sparing implants for companion animals and designing custom implants intended to replace the articulating surfaces of small joints through custom hemiarthroplasty or custom total joint replacement. Little is known about the negative consequences of geometric inaccuracy of custom implants. It appears

likely that geometric inaccuracy would have a negative impact for an implant articulating with another implant (ie, custom total joint arthroplasty) and an implant articulating with native cartilage (ie, custom hemiarthroplasty).

The carpus is a common site of limb-sparing procedures in companion animals. Therefore, the study reported here was conducted on the carpus of cats. We intended to evaluate whether obtaining CT images of a limb with the beam in a sagittal plane would increase geometric accuracy of the articular surface, compared with results for CT images obtained in a longitudinal orientation, considering that there would be a larger number of slices across the articular surface. We hypothesized that measurements for CT images obtained in a transverse orientation would be more accurate than measurements for CT images obtained in a longitudinal orientation. We also intended to compare accuracy of these 2 CT protocols with accuracy for micro-CT of a segment of the entire forelimb that simulated a clinical CT examination with extremely thin slices and with results for laser-scanned articular surfaces after cartilage digestion. We hypothesized that micro-CT measurements would have acceptable accuracy, whereas measurements obtained in longitudinal and sagittal orientations with CT would not have acceptable accuracy. Because our research group was interested in implant design, the focus of the study reported here was to compare geometry of the subchondral bone rather than geometry of the articular surface.

Materials and Methods

Sample

Forelimbs of 12 cats euthanized at 3 local animal shelters for reasons unrelated to the study reported here were harvested and used. Skeletally immature cats (as determined on the basis of results of physical examination or CT) were excluded. Each forelimb was removed in its entirety at the shoulder joint with intact soft tissues. Forelimbs were wrapped in gauze soaked in saline (0.9% NaCl) solution, placed in an extended position in airtight containers, and frozen at –20°C.

An a priori power analysis conducted by use of results for a preliminary experiment performed with 5 specimens revealed that 24 specimens would be needed for the study reported here. Of the 24 specimens harvested, 1 was removed because of skeletal immaturity that was detected after cartilage digestion; thus, the study involved 23 radii. Size of the effects detected in the study were larger than values used for the a priori power analysis; therefore, removal of 1 specimen did not yield a consequential loss in power.

CT images

Forelimbs were thawed at 4°C overnight and then at room temperature (approx 22°C) for 2 hours. Images of thawed forelimbs were obtained by use of a multislice CT scanner[a] with the following settings: 140 mA; 120 kVp; slice thickness, 0.6 mm; slice increment, 0.4 mm; 512 × 512 pixels; and voxel size, 0.6 mm. Images of the entire forelimb were obtained in 2 orientations: longitudinal orientation (CT_{LO} images) with cross-sectional CT data collected in the transverse plane, and transverse orientation (CT_{TO} images) with the cross-sectional CT data collected in the sagittal plane. The transverse orientation was used to maximize the number of slices for articular surface data.

Micro-CT images

A band saw was used to prepare a 4-cm-long section centered over the radiocarpal joint. Specimens were scanned by use of a micro-CT scanner[b] with the following settings: 150 kV; 14.6 W; and voxel size, 0.024 mm.

Laser scans

Enzymatic digestion was used to remove the articular cartilage of the distal portion of the radius without disturbing the subchondral bone.[25] The optimal digestion period was determined in the preliminary experiment. In that experiment, 5 radii of cats were immersed in a papain solution (papain [10 mg/mL], 5.5mM L-cysteine, and 10% penicillin-streptomycin-amphotericin in PBS solution) at 37°C. The bones were dried and weighed at 30 minutes and 2, 6, 12, 18, 24, 36, 48, 60, and 72 hours. There was a negligible change in weight of bones between 36 and 72 hours of digestion. Results of the preliminary experiment indicated that cartilage was removed by 36 hours and that no appreciable bone loss occurred during the 72 hours. Therefore, a 36-hour digestion period was selected.

Carpal joints of the 24 specimens were dissected, and the articular cartilage of the distal portion of the radius was enzymatically digested. Specimens were rinsed with PBS solution, lightly coated with talcum powder, and scanned by use of a laser scanner[c] with an accuracy of 0.025 mm to acquire point clouds of the articular surface of the distal portion of the radius.

Reconstruction and analysis methods

The CT_{LO}, CT_{TO}, and micro-CT images were imported as DICOM images by use of image processing software.[d] The DICOM images were used to reconstruct 3-D models of the radius by use of a marching cubes algorithm. The CT images were filtered and selected to include grayscale values from 226 to 3,053 HU (standard thresholds for bone segmentation). When image manipulation was required to separate the radius from the radial carpal bone and ulna, geometry of the articular surface of the radius was not altered. Micro-CT images were filtered and selected to include all grayscale values > 2,358 HU. Threshold used for the segmentation of micro-CT im-

ages was determined from micro-CT images of the 5 radii obtained during the preliminary experiment and that were segmented at various thresholds. The threshold deemed most accurate for the preliminary study (2,358 HU) was selected for use in the study reported here. Additional steps were not required to isolate the radius from the radial carpal bone and ulna. Output files (.stl format) were generated by use of an optimal generation setting to avoid smoothing or data averaging during processing.

Laser scans were registered to create a single point cloud model for each specimen by use of automatic registration in the modeling software.[e] Outliers and disconnected components were removed prior to creation of .stl files of the laser-scanned bone models; the .stl files of the laser-scanned 3-D point cloud bone models were used as the criterion-referenced standard. The .stl files for CT_{LO}, CT_{TO}, and micro-CT images were compared with the .stl files of the laser-scanned 3-D model point cloud data. Anatomic reference planes (coronal, parasagittal, and transverse) were assigned to each model of the laser scan data by use of computer-aided design software.[f] Bounds of the radial articular surface were determined manually and separated in the computer-aided design software, and coronal, transverse, and parasagittal anatomic planes were aligned with a global coordinate system. The .stl files were imported by use of a high-level programming language[g] into the modeling software.[e] A 2-phase automated best fit alignment of the .stl files of the laser scan, CT_{LO}, CT_{TO}, and micro-CT images was performed. An initial alignment was performed with high-precision fitting and a tolerance of 1×10^{-6} mm. A second alignment was performed with high-precision fitting and fine adjustments to further reduce fitting errors. To evaluate the craniocaudal radius of curvature, planes that were parallel to the parasagittal plane and spaced 0.5 mm apart were created across the articular surface of the laser scan model by use of an automation feature; identical planes were created for the 3-D models of the CT_{LO}, CT_{TO}, and micro-CT images. The radius of curvature was calculated by use of a 2-D measurement feature, with a rectangular box used to determine the bounds of the articular surface and the radius calculation performed by use of the best fit option. Investigators created the rectangular box used to determine the bounds of the articular surface on the basis of the curved region of interest in the criterion-referenced standard of the laser-scan models and duplicated it for all other images by use of the automation feature.

Table 1—Mean ± SD values for measurements obtained from CT, micro-CT, and laser scan images of the articular surface of the distal portion of the radius (n = 23) of 12 feline cadavers*

Variable	Laser scan images	CT_{LO} images	CT_{TO} images	Micro-CT images
ML length				
Length (mm)	12.64 ± 0.92	13.06 ± 0.84	13.13 ± 0.88	12.47 ± 0.81
Difference from laser scan (mm)	NA	0.43[a] ± 0.41[d]	0.49[a] ± 0.41[d]	–0.17[b] ± 0.16[e]
Error (%)	NA	3.62 ± 3.31	4.48 ± 2.59	1.30 ± 1.12
CC length				
Length (mm)	8.37 ± 0.66	8.86 ± 0.67	9.20 ± 0.72	8.34 ± 0.62
Difference from laser scan (mm)	NA	0.49[a] ± 0.20[d]	0.83[b] ± 0.26[d]	–0.03[c] ± 0.10[e]
Error (%)	NA	5.91 ± 2.37	9.97 ± 3.08	0.82 ± 0.86
ML radius of curvature				
Difference from laser scan (mm)	NA	–0.37[a] ± 0.93[d]	–0.31[a] ± 1.15[d]	–0.19[b] ± 0.24[e]
Error (%)	NA	12.04 ± 10.48	14.25 ± 18.06	2.52 ± 2.79
CC radius of curvature				
Difference from laser scan (mm)	NA	2.58[a] ± 22.55[d]	5.48[a] ± 41.99[e]	–0.10[b] ± 0.27[f]
Error (%)	NA	99.41 ± 549.31	256.57 ± 1,716.59	5.18 ± 4.80
Surface deviation				
RMSE (mm)	NA	0.26[a] ± 0.09[d]	0.30[a] ± 0.28[e]	0.04[b] ± 0.02[d]
Maximum positive deviation (mm)	NA	3.04[a] ± 1.17[d]	2.45[a] ± 0.90[d]	0.38[b] ± 0.18[e]
Maximum negative deviation (mm)	NA	–1.18[a] ± 1.11[d]	–1.53[b] ± 0.73[d]	–0.26[c] ± 0.11[e]

*The CT images were obtained in longitudinal orientation (CT_{LO} images) with cross-sectional CT data collected in the transverse plane and in transverse orientation (CT_{TO} images) with cross-sectional CT data collected in the sagittal plane; laser scan images were evaluated with a coordinate measurement machine.

CC = Craniocaudal. ML = Mediolateral. NA = Not applicable. RMSE = Root mean square error.

[a–c]Within a row, mean values with different superscript letters differ significantly ($P < 0.05$).

[d–f]Within a row, SD values with different superscript letters differ significantly ($P < 0.05$).

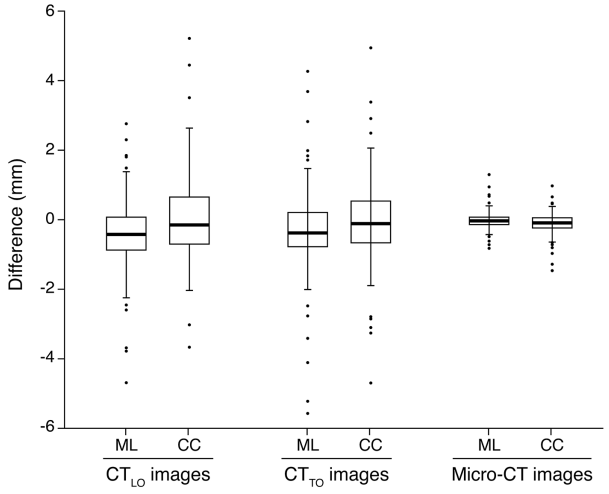

Figure 1—Box-and-whisker plots of differences between measurements derived from CT images obtained in longitudinal orientation (CT_{LO} images) with cross-sectional CT data collected in the transverse plane, CT images obtained in transverse orientation (CT_{TO} images) with cross-sectional CT data collected in the sagittal plane, and micro-CT images and coordinate measurement machine measurements of the mediolateral (ML) and craniocaudal (CC) radius of curvature of the articular surface of the distal portion of the radius of 23 specimens obtained from feline cadavers. All modalities underestimated the ML radius of curvature. The boxes represent the second and third quartiles, the horizontal line in each box represents the median, whiskers represent the highest and lowest values, and circles represent outliers.

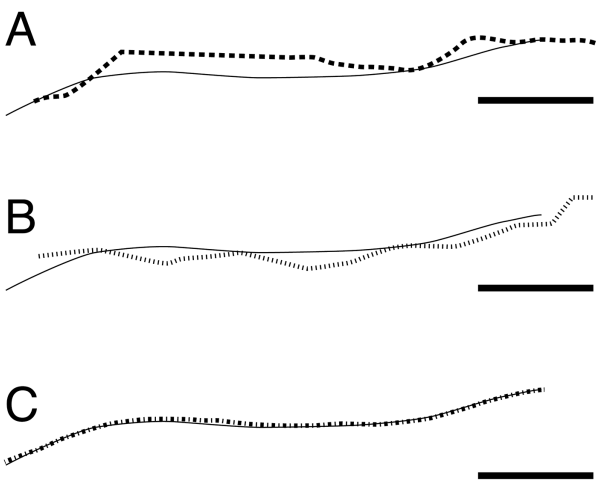

Figure 2—Representative mediolateral cross-sectional measurements of articular joint surfaces of the distal portion of the radius of feline cadavers comparing results for CT_{LO} images (dashed line; A), CT_{TO} images (dotted line; B), and micro-CT images (dashed-and-dotted line; C) with results for a coordinate measurement machine (solid lines). Notice that for CT_{LO} and CT_{TO} images there are large positive and negative deviations from the results for the coordinate measurement machine. In comparison, results for micro-CT images closely approximate results for the coordinate measurement machine. Bar = 1 mm. ***See*** Figure 1 for remainder of key.

Similarly, mediolateral radius of curvature was calculated within planes that were parallel to the coronal anatomic plane and spaced 0.5 mm apart.

Calculations of surface deviations were performed by use of the quality control software[e] in accordance with the same 2-phase best fit alignment described previously. The articular surface of the laser scan point cloud was manually selected, and that region was compared among images by use of a 3-D deviation tool (maximum deviation, 10 mm; maximum angle, 45°) to calculate mean and maximum positive and negative deviations.

The craniocaudal and mediolateral lengths were measured by use of .stl files. The .stl files were imported in the computer-aided design software[f] and aligned by use of an initial manual n-points alignment (3 points on the articular surface and 2 points on the bone shaft), wherein the models for the CT_{LO}, CT_{TO}, and micro-CT images were compared with the model for the laser scan. An additional global alignment was performed by use of an automatic alignment feature (tolerance, 1×10^{-6} mm). Planes parallel to the craniocaudal plane were created at the most dorsal and most palmar aspects of the distal portion of the radius.[26] Planes parallel to the mediolateral plane were created at the most medial and most lateral aspects of the distal portion of the radius. Distance between the most dorsal and most palmar plane was recorded as craniocaudal length, and distance between the most medial and most lateral plane was recorded as the mediolateral length.

Statistical analysis

Accuracy thresholds were selected by extrapolating information from studies[27,28] in which consequences of implant mismatches or articular cartilage steps were described. Accuracy was considered acceptable when the magnitude of the deviation was < 0.6 mm (slice thickness selected for use in the study) for linear dimensions, < 0.75 mm for the radius of curvature,[27] and < 50 µm for mean deviations from the articular surface.

A complete block design statistical model was developed by use of the differences between the images for the various modalities and the laser scan. Residual effects were assumed to have a normal distribution with a mean of 0 and nonequal variance with respect to treatment. A generalized linear mixed model was used to analyze covariance.[h] Values were considered significantly different at $P < 0.05$.

Results

The mean ± SD percentage error was larger for CT_{LO} and CT_{TO} images than micro-CT images for all variables measured **(Table 1)**. Mean mediolateral lengths of CT_{LO}, CT_{TO}, and micro-CT images differed from measurements for the laser scan; however, mean mediolateral lengths did not differ significantly among CT_{LO}, CT_{TO}, and micro-CT images. Mean craniocaudal length differed among CT_{LO}, CT_{TO}, and micro-CT images. Mean error for the mediolateral radius of curvature was larger for CT_{LO} and CT_{TO} images than for micro-CT images **(Figures 1 and 2)**. Mean error for the craniocaudal radius of curvature did not

differ significantly among CT_{LO}, CT_{TO}, and micro-CT images. Root mean square error of the deviation from the articular surface was larger for models of CT_{LO} and CT_{TO} images than for models of micro-CT images **(Figure 3)**. Mean maximum positive surface deviation was larger for CT_{LO} and CT_{TO} images than for micro-CT images. Mean maximum negative surface deviation differed significantly among all CT images; it was smallest for micro-CT images and largest for CT_{TO} images. Variance for micro-CT images was significantly less than variance for CT_{LO} and CT_{TO} images for all variables measured. Significant differences in variance between CT_{LO} and CT_{TO} images were detected for only the craniocaudal radius of curvature, wherein the variance for CT_{TO} images was larger than the variance for CT_{LO} images.

Discussion

For the study reported here, geometry of 3-D models derived from CT_{LO}, CT_{TO}, and micro-CT images were compared with each other and with models derived by use of a laser scanner to assess accuracy. The articular surface of the distal portion of the radius of cats was selected for evaluation because of its small size and curvature, because cadavers of cats euthanatized for reasons unrelated to this study were available for use, and because we anticipated that the geometry of the articular surface of the distal portion of the radius of cats would be more homogeneous than would the articular surface of the distal portion of the radius of dogs, which would require a smaller sample to detect differences in accuracy among CT protocols.

We selected the surface of a laser-scanned image as the criterion-referenced standard. Micro-CT images could have been selected as the criterion-referenced standard. However, 3-D models prepared by use of micro-CT images require image segmentation. Use of thresholds during segmentation influences accuracy of models.[9] However, the preparation of 3-D models from laser-scanned surfaces did not require image segmentation and therefore was independent from scanning parameters and image thresholds. This would be particularly relevant for metaphyseal and subchondral bone, which are locations where cortical bone is thin. Had we opted to use micro-CT images as the criterion-referenced standard for the present study, the micro-CT protocol could have been enhanced by dissection of the radius before micro-CT images were obtained because the bone-air interface would enhance contrast of micro-CT images, compared with contrast for bone interfacing with joint fluid and soft tissues. However, the micro-CT protocol used in the study resembled a protocol used

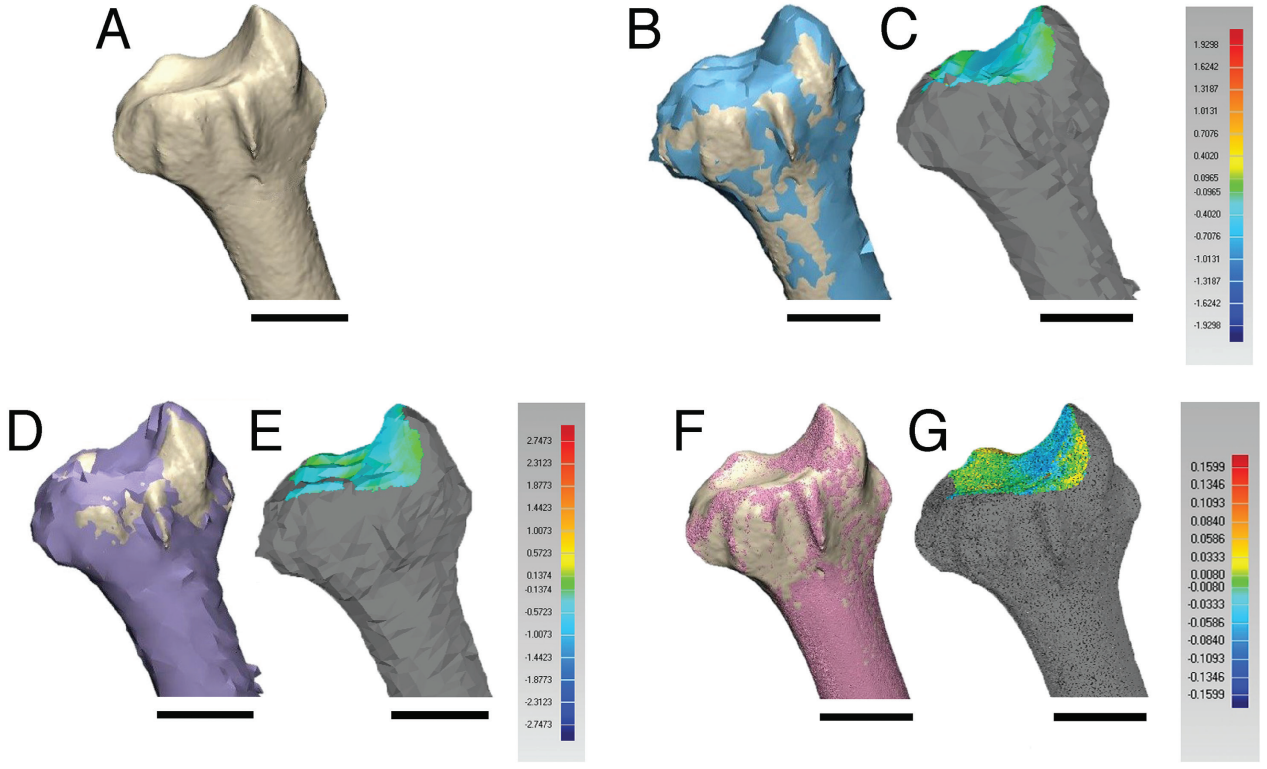

Figure 3—Representative 3-D models (A, B, D, F) and heat maps of deviations from the articular surface (C, E, G) for the radius of a feline cadaver. Positive differences between the models created by use of laser-scanned images (A) and CT_{LO} images (blue areas; B), CT_{TO} images (purple areas; D), and micro-CT images (pink areas; F) are indicated. For the heat maps, negative deviations (light to dark blue) indicate that the CT models overestimated the articular surface, and positive deviations (yellow, orange, or red) indicate that the CT models underestimated the articular surface. Notice that the scale of the heat map differs among panels. Deviations are approximately 10 times as large for the CT_{LO} and CT_{TO} images as for the micro-CT images. Bar = 5 mm.

in clinical settings wherein a segment of the entire limb was scanned. As anticipated, micro-CT was more accurate than conventional CT. However, the use of micro-CT for clinical patients is not feasible because of high amounts of ionizing radiation and slow data acquisition. Other CT methods, including conventional CT with a voxel size < 0.6 mm and cone beam CT, would have provided greater accuracy but were not available in our teaching hospital. High-resolution cone beam CT images have slices as thin as 0.1 mm combined with low radiation, relative to slice thickness and radiation for conventional CT.[29,30]

The distal portion of the radius is a common site of limb-sparing surgery in companion animals[31] and a site of hemiarthroplasty in humans.[32] Accurate assessment of the geometry of joint surfaces is a prerequisite for optimization of articulating custom orthopedic implants (eg, custom arthroplasties or hemiarthroplasties). Accurate fit of articulating surfaces would also require accurate surgical placement of a custom implant. Angular variability and positional variability in joint replacement is improved with surgical navigation implantation[33] and the use of patient-specific alignment instruments.[34] Deviations in measurements of the articular surface (eg, deviations in length or the articular surface) differed among modalities. Accuracy and precision were lower for measurements obtained by use of CT_{LO} and CT_{TO} images, compared with measurements obtained by use of micro-CT images, and most of these differences (4/5 for mean and 5/5 for variance) were significantly different. We accepted the hypothesis that measurements for micro-CT images had acceptable accuracy and that measurements for CT_{LO} and CT_{TO} images did not have acceptable accuracy. The main source of inaccuracy for CT_{LO} and CT_{TO} images was likely a partial volume effect combined with spillover from the adjacent radial carpal bone. The fact that the bone shape was overestimated on CT_{LO} and CT_{TO} images suggested that spillover from the radial carpal bone was most influential. For the micro-CT images, the slight underestimation of dimensions was likely a consequence of the partial volume effect.

The lack of significant differences in mediolateral length among CT_{LO}, CT_{TO}, and micro-CT images may have resulted from the fact that mediolateral length had the largest linear measurements and imaging errors were smallest relative to overall size or to the relatively large variance for measurements of CT_{LO} and CT_{TO} images. Differences in the accuracy for micro-CT images and CT_{LO} or CT_{TO} images were likely a consequence of the increased resolution for the micro-CT images relative to that for the CT_{LO} and CT_{TO} images. Edges of voxels for CT_{LO} and CT_{TO} images were approximately 25 times as large as voxel edges for micro-CT images. Micro-CT images included approximately 15,000 more voxels than CT_{LO} or CT_{TO} images. Dimensions of a voxel comprise in-plane pixel size (a combination of the field of view and matrix dimensions) and slice thickness. A decrease in voxel volume increases geometric accuracy, but it would increase the radiation dose. In a study[35] conducted to evaluate the influence of slice thickness on radiation doses of humans, a decrease in slice thickness increased the radiation dose.

Accuracy and precision of measurements did not differ significantly between CT_{LO} and CT_{TO} images for most linear measures of deviation (3/5 for mean and 5/5 for variance). Therefore, we rejected the hypothesis that use of CT_{TO} images was more accurate than use of CT_{LO} images. Lack of improvement in models created from CT_{TO} images, as compared with CT_{LO} images, was unexpected because there were > 3 times as many slices containing articular surface data for the CT_{TO} images than for the CT_{LO} images. Subjectively, 3-D models reconstructed from the CT_{TO} images had more noise than the CT_{LO} images, likely because of the increased length for x-ray travel within specimens. Beam hardening that appeared to be generated in the region of the elbow joint and radiated along the shaft of the radius to the distal portion of the radius may have been responsible for the lack of an increase in accuracy for CT_{TO} images relative to CT_{LO} images. Beam hardening has been described in the literature.[36] Effects are more pronounced in bone because of the high calcium content[37] and subsequent absorption of x-rays.[38] Attempts to optimize corrections for beam hardening exist in clinical applications[37] and in industrial metrological applications.[38–40] Investigators of another study[41] compared results for CT_{LO}, oblique CT, and CT_{TO} images of a human ankle prosthesis implanted in a stifle joint of a pig. In that study,[41] measurements for CT_{TO} images were less accurate than measurements for CT_{LO} images.

Measurement errors, including errors in the radius of curvature, for models created by use of micro-CT images were small and compatible with the design of conforming implants. By comparison, measurement errors associated with CT_{LO} and CT_{TO} images were large, particularly errors in the radius of curvature measurements. The mediolateral radius of curvature was more accurately evaluated than was the craniocaudal radius of curvature. Additionally, the large percentage errors indicated that although there was no measurement bias (mean differences were centered around zero), the magnitude of error was large, which meant measurements were less reliable. The current resolution for CT_{LO} and CT_{TO} images would not be compatible with the design of custom-conforming arthroplasties or the evaluation of small topographic differences in small articular surfaces. Several studies have been conducted to evaluate the geometric aspects of the accuracy for CT of bones from other species. In a study[42] conducted to compare the accuracy of models of human tibiae created by use of CT images (pixel size, 0.39 X 0.39 mm; slice thickness, 0.6 mm) and MRI scans by use of optical laser scanning, mean of the root mean square error for the entire bone was 0.55 mm, and

mean of the root mean square error for the proximal and distal 10% of the bone was 0.64 and 0.65 mm, respectively. These errors are approximately twice as large as the root mean square error for CT_{LO} and CT_{TO} images in the study reported here. Interestingly, an increase in bone size (human tibia vs cat radius) and a decrease in x-y pixel size did not improve accuracy. In 1 study[43] in which a calibration device with known dimensions was scanned by use of a slice thickness of 1 mm, mean geometric error was 0.17 mm. In another study[23] in which a voxel size of 0.39 × 0.39 × 0.4 mm was used for CT, linear deviation in accuracy for bones of the index finger was 0.21 mm in the distal phalanx, 0.20 mm in the middle phalanx, and 0.19 mm in the proximal phalanx. These error values are similar to the root mean square error values obtained in the study reported here. This likely can be attributed to the fact that human phalanges are similar in size to feline radii. A study[24] conducted to compare the accuracy of length measurements between anatomic landmarks of the vertebral column by use of a CT slice thickness of 1 mm resulted in mean ± SD global error of 1.1 ± 0.8 mm and errors in length measurements ranging from 0.8 to 2.4 mm. These errors are larger than the errors reported for the radii of the present study.

The variables used for CT influence CT accuracy. In a study[8] conducted to evaluate the accuracy of replicas of a canine femur, 3 models were additively manufactured from CT data collected by use of various scan variables, and linear dimensions were compared by use of a touch coordinate measuring system. Various values for penetrability (80 to 140 kVp), tube current (60 to 160 mA), and pitch (0.6 or 0.75), and several retroreconstruction kernels and windows were used. The authors reported that 2% to 29% of the variability was attributable to differences in the model fabrication methods, and 4% to 44% of the variability was attributable to differences in CT scan variables. However, no direct measurements of the 3-D models before manufacturing were collected in that study.[8] In the aforementioned study[23] conducted to evaluate CT accuracy of human phalanges, voxel size was constant (0.12 × 0.12 × 1 mm) but penetrability (80 to 140 kVp) and tube current (80 or 100 mA) varied. However, segmentation thresholds and triangulation resolutions also varied, which complicated the assessment of the influence of CT scan variables on CT accuracy. In that study,[23] investigators compared CT images of the human phalanges to CT images of the additive manufacturing models of the phalanges; however, no comparison was made directly with the bone model. Higher penetrability values resulted in a decrease in the number of voxels in the images of the additive manufacturing models as compared with images of the bones, and an increase in tube current resulted in an increase in voxels in the phalanges but not in the additive manufacturing models. Increases in the lower grayscale threshold resulted in a reduction in the number of voxels in the additive manufacturing model but not in the phalanges and increased the number of voxels in the phalanges but not in the additive manufacturing models. Decreasing the lower threshold resulted in an increase in the number of voxels in the phalanges but not in the additive manufacturing model.[44] These changes illustrate the large influence that CT variables and segmentation have on the accuracy of CT data.

Investigators have used segmentation based on grayscale value filtering.[8,9] Alternative segmentation strategies, including Canney edge detection and intensity thresholding, have been described. A study[44] was conducted to compare CT images (pixel size, 0.39 × 0.39 mm; slice thickness, 0.5 mm) and 3-D contact scans of ovine femurs. Mean deviation was 0.24 mm for single threshold errors and 0.18 mm for multithreshold errors. Deviations in that study[44] were similar to deviations in the study reported here. On the basis of the variety of scanning variables and segmentation methods available for use, acceptable scanning variables and segmentation methods for modeling of small joint surfaces will likely require comprehensive standardization of CT imaging protocols, retroreconstruction methods, and segmentation to optimize CT accuracy for specific regions of interest.

Optimizing CT accuracy is important when patient-specific computer-aided design data are used in the design of hemiarthroplasty implants. Increasing the conformity of a hemiarthroplasty can reduce friction and improve wear performance, as compared with in vivo wear.[45] In hip joint hemiarthroplasty, undersize of the radius of a prosthetic head by as little as 0.75 mm (6.25%) negatively impacts the performance of the hemiarthroplasty.[27] The large difference in maximum positive deviation and negative deviation and in radius of curvature among modalities in the present study warrants further investigation into the optimal data collection methods that can be used to accurately record the articular surface of feline radiocarpal joints and other small joints. Currently, evaluations conducted to assess the effect of articular surface geometry on cartilage contact stresses relies on finite-element modeling.[14,15]

Clinical CT imaging and grayscale filtering segmentation methods used to develop 3-D models in the study reported here did not have sufficient geometric accuracy for modeling small articular surfaces for the purpose of designing a surface that would conform to an articular surface, such as the surface of a prosthesis intended for hemiarthroplasty. Lack of accuracy of clinical CT imaging raises concerns about the potential lack of accuracy when planning the correction of a limb deformity or repair of an articular fracture. Streamlined protocols for imaging, segmentation, and smoothing should be developed to optimize CT accuracy.

Acknowledgments

This manuscript represents a portion of the dissertation submitted by Dr. Webster to the Edward P. Fitts Department of Indus-

trial and Systems Engineering as partial fulfillment of the requirements for a Doctor of Philosophy degree.

Supported by the Leonard X. Bosack & Betty M. Kruger Charitable Foundation.

The authors declare that there were no conflicts of interest.

The authors thank Dr. Susan Bernacki, Dr. Ian Robertson, Dr. Harvey West II, James Robey, Jimmy Thostenson, Amanda Hanley, Diana Courtright, and Kristen Karasiewicz for technical assistance.

Footnotes

a. Siemens Sensation 64, Siemens, Washington, DC.
b. XT H 225 ST, Nikon, Melville, NY.
c. FARO Edge ScanArm, FARO, Lake Mary, Fla.
d. Mimics, version 17.0, Materialise, Plymouth, Mich.
e. Geomagic Studio, 3D Systems, Rock Hill, SC.
f. 3-matic, version 9, Materialise, Plymouth, Mich.
g. Python script, Python Software Foundation, Wilmington, Del.
h. COVTEST, PROC GLIMMIX, SAS, version 10.4, SAS Institute Inc, Cary, NC.

References

1. Hui C, Pi Y, Swami V, et al. A validation study of a novel 3-dimensional MRI modeling technique to identify the anatomic insertions of the anterior cruciate ligament. *Orthop J Sports Med* 2016;4:2325967116673797.
2. Chang EY, Moses DA, Babb JS, et al. Shoulder impingement: objective 3D shape analysis of acromial morphologic features. *Radiology* 2006;239:497–505.
3. Prevrhal S, Fox JC, Shepherd JA, et al. Accuracy of CT-based thickness measurement of thin structures: modeling of limited spatial resolution in all three dimensions. *Med Phys* 2003;30:1–8.
4. Viegas SF, Hillman GR, Elder K, et al. Measurement of carpal bone geometry by computer analysis of three-dimensional CT images. *J Hand Surg Am* 1993;18:341–349.
5. Lalone EA, Willing RT, Shannon HL, et al. Accuracy assessment of 3D bone reconstructions using CT: an intro comparison. *Med Eng Phys* 2015;37:729–738.
6. Zhang ZL, Cheng JG, Li G, et al. Detection accuracy of condylar bony defects in Promax 3D cone beam CT images scanned with different protocols. *Dentomaxillofac Radiol* 2013;42:20120241.
7. Bois AJ, Fening SD, Polster J, et al. Quantifying glenoid bone loss in anterior shoulder instability: reliability and accuracy of 2-dimensional and 3-dimensional computed tomography measurement techniques. *Am J Sports Med* 2012;40:2569–2577.
8. Fitzwater KL, Marcellin-Little DJ, Harrysson OLA, et al. Evaluation of the effect of computed tomography scan protocols and freeform fabrication methods on bone biomodel accuracy. *Am J Vet Res* 2011;72:1178–1185.
9. Pinto JM, Arrieta C, Andia ME, et al. Sensitivity analysis of geometric errors in additive manufacturing medical models. *Med Eng Phys* 2015;37:328–334.
10. Chen X, Zimmerman BK, Lu XL. Determine the equilibrium mechanical properties of articular cartilage from the short-term indentation response. *J Biomech* 2015;48:176–180.
11. Varga P, Schefzig P, Unger E, et al. Finite element based estimation of contact areas and pressures of the human scaphoid in various functional positions of the hand. *J Biomech* 2013;46:984–990.
12. Márquez-Florez K, Vergara-Amador E, de Las Casas EB, et al. Theoretical distribution of load in the radius and ulna carpal joint. *Comput Biol Med* 2015;60:100–106.
13. Majors BJ, Wayne JS. Development and validation of a computational model for investigation of wrist biomechanics. *Ann Biomed Eng* 2011;39:2807–2815.
14. Klennert BJ, Ellis BJ, Maak TG, et al. The mechanics of focal chondral defects in the hip. *J Biomech* 2017;52:31–37.
15. Hui-Hui W, Dong W, An-Bang M, et al. Hip joint geometry effects on cartilage contact stresses during a gait cycle. *Conf Proc IEEE Eng Med Biol Soc* 2016;2016:6038–6041.
16. Katz MA, Beredjiklian PK, Bozentka DJ, et al. Computed tomography scanning of intra-articular distal radius fractures: does it influence treatment? *J Hand Surg Am* 2001;26:415–421.
17. Leventhal EL, Wolfe SW, Moore DC, et al. Interfragmentary motion in patients with scaphoid nonunion. *J Hand Surg Am* 2008;33:1108–1115.
18. Márquez-Florez K, Vergara-Amador E, Gavilan-Alfonso M, et al. Load distribution on the radio-carpal joint for carpal arthrodesis. *Comput Methods Programs Biomed* 2016;127:204–215.
19. Soslowsky LJ, Flatow EL, Bigliani LU, et al. Articular geometry of the glenohumeral joint. *Clin Orthop Relat Res* 1992;285:181–190.
20. Breit S, Pfeiffer K, Pichler R. Use of a 3D laser scan technique to compare the surface geometry of the medial coronoid process in dogs affected with medial compartment disease with unaffected controls. *Vet J* 2010;185:285–291.
21. Wilson LAB, Humphrey LT. A virtual geometric morphometric approach to the quantification of long bone bilateral asymmetry and cross-sectional shape. *Am J Phys Anthropol* 2015;158:541–556.
22. Trinh NH, Lester J, Fleming BC, et al. Accurate measurement of cartilage morphology using a 3D laser scanner. In: Beichel RR, Sonka M, eds. *Computer vision approaches to medical image analysis*. Berlin: Springer-Verlag, 2006;37–48.
23. DeVries NA, Gassman EE, Kallemeyn NA, et al. Validation of phalanx bone three-dimensional surface segmentation from computed tomography images using laser scanning. *Skeletal Radiol* 2008;37:35–42.
24. Aubin CÉ, Dansereau J, Parent F, et al. Morphometric evaluations of personalised 3D reconstructions and geometric models of the human spine. *Med Biol Eng Comput* 1997;35:611–618.
25. Clark JM, Huber JD. The structure of the human subchondral plate. *J Bone Joint Surg Br* 1990;72:866–873.
26. Dunlap AE, Mathews KG, Walters BL, et al. Three-dimensional assessment of the influence of juvenile pubic symphysiodesis on the pelvic geometry of dogs. *Am J Vet Res* 2018;79:1217–1225.
27. Harris WH, Rushfeldt PD, Carlson CE, et al. Pressure distribution in the hip and selection of hemiarthroplasty, in *Proceedings*. 3rd Open Sci Meet Hip Soc, 1975;93–98.
28. Baratz ME, Des Jardins J, Anderson DD, et al. Displaced intra-articular fractures of the distal radius: the effect of fracture displacement on contact stresses in a cadaver model. *J Hand Surg Am* 1996;21:183–188.
29. Van Dessel J, Nicolielo LF, Huang Y, et al. Quantification of bone quality using different cone beam computed tomography devices: accuracy assessment for edentulous human mandibles. *Eur J Oral Implantol* 2016;9:411–424.
30. Cao Q, Zbijewski W, Sisniega A, et al. Multiresolution iterative reconstruction in high-resolution extremity cone-beam CT. *Phys Med Biol* 2016;61:7263–7281.
31. Liptak JM, Dernell WS, Ehrhart N, et al. Cortical allograft and endoprosthesis for limb-sparing surgery in dogs with distal radial osteosarcoma: a prospective clinical comparison of two different limb-sparing techniques. *Vet Surg* 2006;35:518–533.
32. Herzberg G, Burnier M, Marc A, et al. Primary wrist hemiarthroplasty for irreparable distal radius fracture in the independent elderly. *J Wrist Surg* 2015;4:156–163.
33. Beckmann J, Stengel D, Tingart M, et al. Navigated cup implantation in hip arthroplasty. *Acta Orthop* 2009;80:538–544.
34. Ast MP, Nam D, Haas SB. Patient-specific instrumentation for total knee arthroplasty: a review. *Orthop Clin North Am* 2012;43:e17–e22.
35. Cohnen M, Poll LW, Puettmann C, et al. Effective doses in standard protocols for multi-slice CT scanning. *Eur Radiol* 2003;13:1148–1153.

36. Brooks RA, Chiro GD. Beam hardening in x-ray reconstructive tomography. *Phys Med Biol* 1976;21:390–398.
37. Joseph PM, Ruth C. A method for simultaneous correction of spectrum hardening artifacts in CT images containing both bone and iodine. *Med Phys* 1997;24:1629–1634.
38. Tan Y, Kiekens K, Welkenhuyzen F, et al. Simulation-aided investigation of beam hardening induced errors in CT dimensional metrology. *Meas Sci Technol* 2014;25;064014.
39. Zhang X, Li L, Zhang F, et al. Improving the accuracy of CT dimensional metrology by a novel beam hardening correction method. *Meas Sci Technol* 2015;26:1–11.
40. Krumm M, Kasperl S, Franz M. Reducing non-linear artifacts of multi-material objects in industrial 3D computed tomography. *NDT Int* 2008;41:242–251.
41. Kohonen I, Koivu H, Vahlberg T, et al. Total ankle arthroplasty: optimizing computed tomography imaging protocol. *Skeletal Radiol* 2013;42:1507–1513.
42. Rathnayaka K, Sahama T, Schuetz MA, et al. Effects of CT image segmentation methods on the accuracy of long bone 3D reconstructions. *Med Eng Phys* 2011;33:226–233.
43. Eggers G, Klein J, Welzel T, et al. Geometric accuracy of digital volume tomography and conventional computed tomography. *Br J Oral Maxillofac Surg* 2008;46:639–644.
44. Van den Broeck J, Vereecke E, Wirix-Speetjens R, et al. Segmentation accuracy of long bones. *Med Eng Phys* 2014;36:949–953.
45. McCann L, Ingham E, Jin Z, et al. An investigation of the effect of conformity of knee hemiarthroplasty designs on contact stress, friction and degeneration of articular cartilage: a tribological study. *J Biomech* 2009;42:1326–1331.